

Ni-Cu bimetallic catalytic system for producing HMF-derived value-added biofuels

Nerea Viar^a, Jesus Maria Requies^a, Ion Agirre^a, Aitziber Iriondo^a, Miryam Gil-Calvo^a, Pedro Luis Arias^a

^a Chemical and Environmental Engineering Department. Engineering Faculty of Bilbao, University of Basque Country (UPV/EHU), Plaza Ingeniero Torres Quevedo 1 – 48013 Bilbao (Spain)

Email: nerea.viar@ehu.eus

ABSTRACT: Biomass is the only renewable carbon source capable of replacing conventional production of chemicals and fuels derived from non-renewable resources. The cellulose monomers derived from lignocellulosic biomass can be transformed into 5-hydroxymethylfurfural (HMF), which can be further converted into 2,5-dimethylfuran (DMF) and 2,5-dimethyltetrahydrofuran (DMTHF). These products can be used as substitutes for standard gasoline or as additives. This study has shown that by using Ni-Cu catalysts supported on ZrO₂, DMF can be obtained with a yield of 70 % after 25 hours on stream. Experiments were carried out in a continuous fixed-bed reactor, and complete HMF conversion was achieved by the formation of Ni-Cu species. The importance of Ni active sites in the hydrogenation of DMF to obtain DMTHF was shown, observing how the progressive Ni oxidation phenomenon during the reaction favors DMF production to the detriment of DMTHF. Catalyst evolution was corroborated by different characterization techniques after carrying out several experiments with different durations.

KEYWORDS *Bimetallic catalyst, Ni-Cu, DMF, DMTHF, hydrogenolysis.*

INTRODUCTION

Research into new renewable and sustainable resources is called for due to the depletion of fossil fuel reserves, rise of anthropogenic CO₂ emissions, and increase in energy demand.¹⁻³ Accordingly, lignocellulosic biomass has received increased interest as a potential energy source due to its possible conversion into high value-added biofuels and chemicals, which can have a low (potentially zero) carbon footprint.¹ Among all the products/intermediates that can be obtained from lignocellulosic biomass, 5-hydroxymethylfurfural (HMF) is an interesting target product; this compound is included within the “Top 10+4” biobased building block products listed by Bozell and Petersen.⁴ This molecule is obtained from C₆ carbohydrates, and can be transformed into a versatile range of products, such as ethoxymethylfurfural (EMF), 2,5-furandicarboxylic acid (FDCA), furfuryl alcohol (FFA), formic acid (FA), 2,5-diformylfuran (DFF), and 2,5-dimethylfuran (DMF).⁵⁻⁷ Among these furan derivatives, DMF and 2,5-dimethyltetrahydrofuran (DMTHF) are considered to be good candidates for replacing conventional fuels due to their high octane number and energy density, elevated boiling point, and low solubility in water.⁸⁻¹²

Extensive research has been carried out to develop a suitable catalytic system for producing DMF from lignocellulosic biomass. Most studies have focused on discontinuous

processes using noble and non-noble metal-based catalysts in batch-type reactors. Priezel et al.¹³ have synthesized a complex ruthenium-based catalyst supported on carbon nanotubes, optimizing the DMF yield to 83.5 % after 1 h of reaction time at 150 °C and 20 bar of H₂. To avoid the use of noble metals, Li et al.¹⁴ have employed a bifunctional Co-CoO_x catalyst, where Co acts as the metal, while CoO_x provides the required acidity. Use of this catalyst led to a DMF yield of 83.3 % at 170 °C after 12 h of reaction time. The use of an iridium and platinum-based bimetallic catalyst has been investigated by Ledesma and colleagues.¹⁵ The high dispersion of bimetallic nanoparticles and the neutral nature of the support are critical aspects for the efficient production of DMF (86 % yield) after 4 h of reaction time at 120 °C and 15.2 bar of H₂ pressure.

The catalytic production of DMTHF has gained more attention in recent years. As in the case of DMF, most studies have been performed in discontinuous systems. Xiao et al.¹⁶ have developed a complex catalytic system based on Ni nanoparticles inlaid into Ni phyllosilicate. The synergy between the nanoparticles and Ni phyllosilicate structure produces high DMF and DMTHF yields. Kumalaputri et al.¹⁷ have used a Cu- and ruthenium-based catalyst for realizing an 80 % yield for both DMF and DMTHF at 220 °C and 50 bar of H₂ pressure. Recently, Li and co-workers¹¹ have investigated a biphasic tandem catalytic process to

obtain DMTHF from fructose. On the one hand, the aqueous phase contains H_2SO_4 as a Brønsted acid homogeneous catalyst, and, on the other hand, the organic phase contains a Pd/AC heterogeneous catalyst for optimizing the production of DMTHF. A maximum DMTHF yield of 70 % was obtained after 12 h of reaction time at 220 °C using diethyl ether as organic solvent.

According to this background and considering the lack of research data for continuous systems, this study focuses on the production of DMF and DMTHF using a continuous fixed-bed reactor for a prolonged time on stream (25 hours). This type of continuous process provides higher efficiencies, lower production costs,¹⁸ and is preferable for use on an industrial scale. Moreover, non-noble metal-based catalysts have been studied to minimize production costs. Furthermore, bimetallic catalysts have been synthesized to optimize the production of the desired products by exploiting the possible interaction between the two metals. Thus, apart from the activity of the different catalysts, this study reveals their stability, providing a more realistic view of the behavior of catalytic systems in HMF hydrogenolysis for obtaining biofuels such as DMF and DMTHF.

EXPERIMENTAL

DMF and DMTHF production

The production of DMF and DMTHF was carried out in a continuous fixed-bed reactor in the vapor phase, operating under a H_2 atmosphere of 15 bar and a temperature of 275 °C. The catalyst was reduced before the beginning of the reaction, while working up to the reaction operating conditions.¹⁹ Synthetic HMF (Sigma-Aldrich, 99 %) diluted in 1-butanol (1.5 wt%) was fed into the reactor by a HPLC pump. The weight hour space velocity (WHSV) (g HMF/g cat h) in this reaction was 0.15 h^{-1} .

Activity results are explained by HMF conversion and the DMF/DMTHF yield, which are defined as follows:

$$\text{Conversion (\%)} = \frac{N_{\text{HMF}}^{\text{in}} - N_{\text{HMF}}^{\text{out}}}{N_{\text{HMF}}^{\text{in}}} \cdot 100 \quad (1)$$

$$\text{Yield (\%)} = \frac{N_{\text{DMF/DMTHF}}^{\text{out}}}{N_{\text{HMF}}^{\text{in}}} \cdot 100 \quad (2)$$

where N is the molar flow rate given as mol/min.

Analysis of liquid streams

Liquid and gas chromatography was employed to analyze the feed and the liquid product streams, respectively. More specifically, a high-performance liquid chromatograph (HPLC 1260 Infinity equipped with a Hi-Plex H column and infrared detector) was used to analyze HMF, while DMF, DMTHF and the other byproducts were determined by a gas chromatograph (Agilent 6804 GC equipped with a flame ionization detector (FID) and using a SupraWax 280 capillary column).

Catalyst preparation

Bimetallic catalysts supported on ZrO_2 were prepared by wetness impregnation. $\text{ZrO}(\text{NO}_3)\cdot\text{H}_2\text{O}$ (Sigma-Aldrich,

99 %), $\text{Cu}(\text{NO}_3)_2\cdot\text{H}_2\text{O}$ (Alfa Aesar, 98 %), and $\text{Ni}(\text{NO}_3)_2\cdot 6\text{H}_2\text{O}$ (Sigma-Aldrich, 99.999 %) were used as reagents.

The impregnation method was conducted in two different ways: i) co-impregnation of both metals, Ni and Cu, in a single step that involved mixing together Zr, Ni and Cu nitrates, and ii) two-step impregnation of the metals. In the first case, both metals were impregnated in the same step, and then the catalyst was dried and calcined in air at 250 °C for 2 h. In the second case, an initial drying and calcination step was carried out after the first metal impregnation (under the same conditions as above), and, then, the second metal was impregnated. After the second impregnation, the catalyst was dried and calcined under the same conditions. In this last procedure, the catalyst was calcined twice.

The co-impregnated catalysts are YNiXCuZr , where Y and X refer to the nominal weight of Ni and Cu, respectively. On the other hand, the catalysts prepared in two steps are YNi-XCuZr , where Cu is first impregnated, and XCu-YNiZr , where Ni is impregnated first.

Finally, the ZrO_2 support was synthesized for its characterization. Zr nitrates were calcined at 250 °C for 2 h.

Catalyst characterization

The textural and physico-chemical properties of the prepared bimetallic catalysts were determined by different characterization techniques: N_2 physisorption (BET method to determine the surface area), Inductively Coupled Plasma Optical Emission Spectroscopy (ICP-OES), Temperature Programmed Reduction with hydrogen (H_2 -TPR), Temperature Programmed Desorption with ammonia (NH_3 -TPD), X-ray Diffraction (XRD), Scanning Transmission Electron Microscopy (STEM) and X-ray Photoelectron Spectroscopy (XPS).

Textural properties

N_2 adsorption-desorption isotherms were obtained at -198 °C after outgassing the calcined samples at 150 °C using an Autosorb®-1-C/TCD (Quantachrome, USA). The isotherms obtained were used to measure the BET surface area, pore volume, and average pore diameter.

Inductively Coupled Plasma Optical Emission Spectroscopy (ICP-OES)

The calcined catalysts were first dissolved in an acid solution (75 % HCl and 25 % HNO_3 , in volume) using an ETHOS 1, a Milestone microwave digestion system. The metal content was then determined by ICP-OES (Perkin-Elmer Optima 3300DV).

Temperature Programmed Reduction with hydrogen (H_2 -TPR)

The reducibility of the catalysts was studied by an AutoChem II Instrument (Micromeritics, USA) equipped with a TCD detector. The calcined catalysts were pretreated in situ, heating the sample to 200 °C with He to desorb the physisorbed impurities. The samples were then cooled to

50 °C, and again heated to 850 °C at a rate of 10 °C/min by flowing a reducing gas (5 % v/v H₂ diluted in Ar).

Temperature Programmed Desorption with ammonia (NH₃-TPD)

Catalyst acidity was examined by an AutoChem II Instrument (Micromeritics, USA) equipped with a TCD detector. The calcined samples were reduced by flushing H₂ (5 % v/v H₂ diluted in Ar) at 275 °C for 1 h at the same temperature, and the physisorbed impurities were desorbed by flowing He for 30 min. The catalysts were then cooled to 100 °C, and NH₃ (10 % v/v NH₃ diluted in He) was fed to the sample for 30 min. The physisorbed NH₃ was subsequently removed by increasing the sample temperature to 150 °C with He for 60 min. Finally, the chemisorbed NH₃ was detected by the TCD by heating the samples to 850 °C with He at a rate of 10 °C/min.

X-ray Diffraction (XRD)

X-ray diffraction patterns for the fresh-reduced and used catalysts were obtained by using a Seifert XRD 3000 diffractometer equipped with a PW 2200 Bragg-Brentano $\theta/2\theta$ goniometer, bent graphite monochromator, and automatic slit, using Cu K radiation (0.15418 nm) and 0.028° steps for scanning. The average crystallite size was calculated using the Scherrer equation.

Scanning Transmission Electron Microscopy (STEM)

Elemental maps for the reduced samples were obtained to calculate the mean particle size of the catalysts. On the one hand, a FEI Titan Cubed G2 60-300 transmission electron microscope at 300 kV was used, equipped with a Schottky X-FEG field emission electron gun, a monochromator, and a CEOS GmbH spherical aberration (Cs) corrector on the image side. On the other hand, a Super-X

EDX system was used under a high-angle annular dark-field (HAADF) detector for Z contrast imaging under STEM conditions (camera length of 115 mm) using a pixel size of 2 nm, a dwell time of 900 s, and an image size of 512 x 512 pixels. The TEM samples were prepared by dispersion into an ethanol solvent and maintaining the suspension in an ultrasonic bath for 15 min. A drop of suspension was then spread onto a TEM Cu grid (300 Mesh) covered by a perforated carbon film, followed by drying under vacuum. In addition, EDX microanalyses were carried out with a Super-X EDX system, using a probe current of 240 pA and a semi-convergence angle of 10 mrad. HAADF STEM images were collected with an inner detector radius of 63.5 mrad.

X-ray Photoelectron Spectroscopy (XPS)

Reduced and used catalysts were studied by this characterization technique to analyze the surface (oxidation state, atomic ratios, and interactions of the species formed) using a VG Escalab 200R spectrometer equipped with a hemispherical electron analyzer and an Al K α (h = 1486.6) 120 W X-ray source. A stainless-steel sample holder was used to deposit the samples. First, the samples were degassed at 300 °C in a pre-treatment chamber. The spectrometer base pressure was typically 9-10 torr (0.0133 bar). The spectra were collected with a pass energy of 20 eV, which is usually considered a high-resolution condition.

RESULTS AND DISCUSSION

Catalysts characterization results

Chemical and textural properties

Table 1 summarizes the textural properties and metal loading for the prepared catalysts determined from the N₂ adsorption-desorption and ICP-OES characterization techniques, respectively.

Table 1: Chemical and textural properties for the calcined support and catalysts

Group	Catalyst	BET ^a (m ² /g)	Pore volume ^a (cm ³ /g)	Average pore diameter ^a (nm)	Cu ^b (%)	Ni ^b (%)
Support	ZrO ₂	137.6	0.267	7.2	-	-
Monometallic	15CuZr	35.1	0.094	10.7	13.0	-
	15NiZr	5.0	0.033	25.3	-	10.8
Bimetallic (one-step impregnation)	7Ni7CuZr	5.5	0.048	32.1	5.3	5.9
	15Ni7CuZr	18.3	0.034	7.4	4.1	10.0
	15Ni15CuZr	18.1	0.034	7.7	12.4	13.2
	30Ni15CuZr	77.0	0.042	3.8	8.4	18.7
Bimetallic (two-step impregnation)	15Cu-15NiZr	18.5	0.134	29.6	10.8	8.5
	15Ni-15CuZr	12.3	0.031	10.0	8.0	11.5
	15Cu-30NiZr	30.0	0.024	4.2	18.3	22.0
	30Ni-15CuZr	18.0	0.017	5.2	11.8	30.2

^a Obtained from N₂-physisorption ^b from ICP-OES

The calcined ZrO₂ support showed the highest BET surface area and pore volume. These values decreased when Ni and/or Cu were impregnated because the porous structure of the support was blocked by metal deposition.²⁰⁻²² Comparing the monometallic catalysts, the 15NiZr catalyst

showed a smaller surface area than the 15CuZr, which can be attributed to the blocking of the pores by the metallic Ni clusters present on the surface. In turn, this can be associated with the low dispersion of the metal.²¹ Meanwhile,

in the case of the Cu monometallic catalyst, the metal species can be more dispersed in the support. In the case of bimetallic catalysts, the alternative method of impregnating first with Ni and then Cu provided a higher surface area, suggesting a better dispersion for the metals.

Regarding the metal loading of the catalysts, the experimental value was found to be lower than the nominal content in most cases, and this difference became greater as the metal loading was increased. For bimetallic catalysts prepared by one-step impregnation, the incorporation of higher Ni loading (keeping the nominal Cu loading constant) meant lower Cu loadings. In the case of bimetallic catalysts impregnated in two steps, the second metal was better impregnated than the first, leading to a higher Cu loading when Ni was impregnated first, and a higher Ni loading when Cu was impregnated first. In these catalysts, in contrast to one-step impregnated catalysts, impregnating higher Ni loadings (keeping the nominal Cu loading constant) provided higher Cu loadings. Finally, it should be noted that the average pore diameter was higher than that in the support in some cases, especially for the 7Ni7CuZr and 15Cu-15NiZr catalysts. This suggests that the smaller pores were filled by the incorporated metals, involving an increase in the average pore diameter.²³

Reducibility

The H₂-TPR profiles and their deconvolution for the monometallic and bimetallic catalysts are summarized in Figure 1 and Figure 2, respectively. The monometallic 15CuZr catalyst recorded three different peaks at temperatures of 195 °C, 205 °C and 240 °C. Similarly, monometallic 15NiZr registered different peaks at higher temperatures (270 °C, 300 °C and 380 °C). Reports in the literature indicate that highly dispersed particles and those particles interacting weakly with the support record lower reduction temperatures. In contrast, bulk NiO and CuO and particles interact strongly with the support, recording high reduction temperatures.^{18,24,25}

The H₂-TPR profiles for the bimetallic catalysts can also be deconvoluted into three reduction peaks (see Figure 2). When compared to the monometallic 15NiZr catalyst, all of the peaks are shifted to lower temperatures. This observation seems to indicate that Cu facilitates the reducibility of Ni.²⁶⁻²⁸ According to the literature,²⁰ the first peak is related to the reduction of the Cu⁺² species, and the last peak to Ni⁺² reduction, while the intermediate peak (in blue) could be associated with the reduction of Ni-Cu species. Table 2 presents a summary of the peak temperature and contribution obtained from the deconvolution.

Based on the results presented in Figure 2 and Table 2, the bimetallic catalysts impregnated in one step generally recorded a lower contribution for Ni-Cu reduction compared to samples prepared by the two-step method. This suggests that impregnating metals in sequential steps can promote higher interaction between Ni and Cu species. Furthermore, in the case of the one-step impregnation of

bimetallic catalysts, it seems that an increase in metal loading leads to a better reducibility for the catalyst (see Figure 2). The 7Ni7CuZr catalyst recorded the highest temperature peak at 335 °C, while, for the 30Ni15CuZr catalyst, this temperature peak decreased to 250 °C. The difference in the reduction temperature can be attributed to a weaker metal support interaction in the latter catalyst, leading to lower reduction temperatures when metal loading is increased.^{18,29}

Interesting results were found when analyzing the H₂-TPR profiles for those catalysts impregnated in two steps; the reduction temperature differs depending on the impregnation sequence for the metals. Specifically, a better reducibility was observed when Ni was impregnated in a second step (highest temperature peak: 215 °C for the 15Ni-15CuZr catalyst, and 235 °C for the 30Ni-15CuZr catalyst) (see Figure 2), while a higher reduction temperature was detected when Ni was impregnated first (250 °C for the 15Cu-15NiZr catalyst and 310 °C for the 15Cu-30NiZr catalyst). According to the literature,³⁰ the metal impregnated in the first step records a stronger interaction with the support. When impregnating Ni first, there is a higher interaction between Ni and ZrO₂, resulting in a higher reduction temperature. Moreover, impregnating Ni in the second step meant a higher contribution, and, therefore, higher interaction between both metals. Finally, higher Ni loading also involved higher interaction between Ni and Cu.

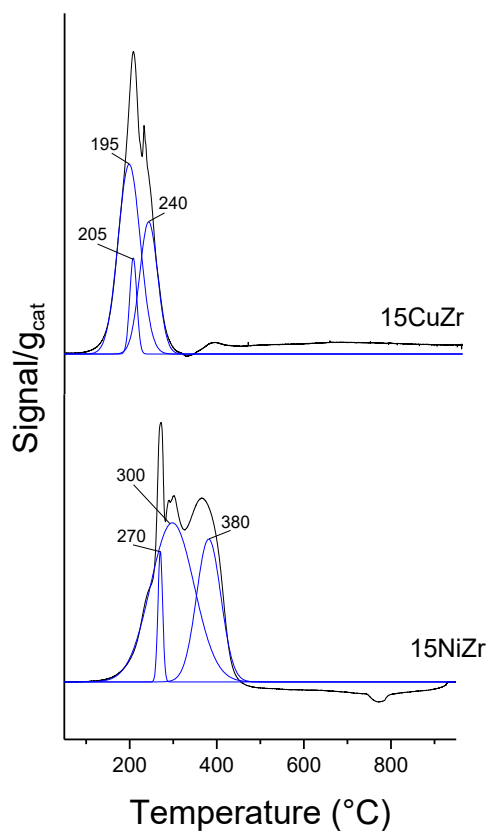


Figure 1: H₂-TPR profiles for the monometallic catalysts

Acidic properties

The acidic properties were studied by NH_3 -TPD. Some authors have reported that high acidity favors C-C bond cleavage, leading to the formation of degradation and/or ring-opening products.^{31,32} This phenomenon needs to be avoided in this reaction. Table 3 shows that the ZrO_2 support had low acidity, with a value of 0.39 mmol $\text{NH}_3/\text{g}_{\text{cat}}$. In the case of monometallic catalysts, acidity decreased when Cu was loaded onto the support. The incorporated Cu particles could be partially covering acid sites on the support, thus decreasing the catalyst's total acidity.^{33,34} However, the addition of Ni considerably increased this acidity. It seems that the high acidity detected for the monometallic 15NiZr catalyst was related to the presence of Lewis acid sites associated with the presence of Ni^{2+} .³⁵ This is in good agreement with the H_2 -TPR results, where higher temperatures are needed to reduce this catalyst, involving the formation of Ni^{+2} species with stronger interaction with the support that can also act as Lewis acid sites.

The acidity calculated for the bimetallic catalysts was similar to or lower than that of the support, except for the 7Ni7CuZr catalyst. In this last case, a similar effect to that found for the monometallic Ni catalyst may be taking place. The harder reducibility of this sample, as observed from the H_2 -TPR profiles, can be explained by the formation of Ni^{+2} species that strongly interact with the support and act as Lewis acid sites.³⁶ This fact is also in good agreement with the XPS results, where the $\text{Ni}^0/\text{Ni}^{+2}$ for the fresh-reduced catalyst is low when compared to the other bimetallic catalysts. The remaining bimetallic catalyst prepared in a single step recorded comparable or slightly lower acidity values compared to the support. In the case of the bimetallic catalyst impregnated in two steps, the acidity was found to be even lower, except for the 15Cu-15NiZr catalyst. The double calcination of these latter catalysts can obviously favor a decrease in the number of acid sites.

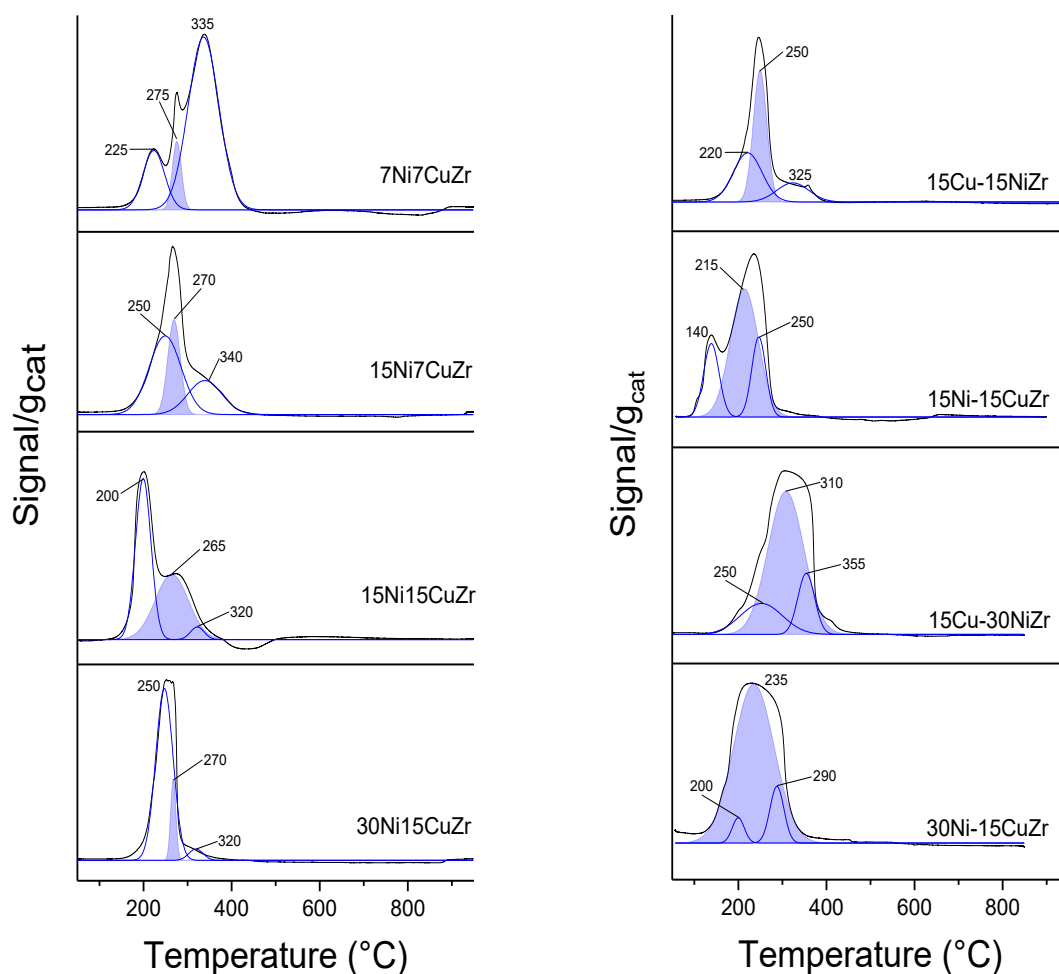


Figure 2: H_2 -TPR profiles for the bimetallic catalysts

Table 2: Deconvolution of H₂-TPR profiles (maximum temperature of the reduction peaks and contribution in area %)

Group	Catalyst	Cu		Ni-Cu		Ni	
		T (°C)	Contribution (%)	T (°C)	Contribution (%)	T (°C)	Contribution (%)
Bimetallic (one-step impregnation)	7Ni7CuZr	225	18	275	9	335	74
	15Ni7CuZr	250	52	270	24	340	24
	15Ni15CuZr	200	52	265	45	320	4
	30Ni15CuZr	250	84	270	12	320	5
Bimetallic (two-step impregnation)	15Cu-15NiZr	220	37	250	47	325	16
	15Ni-15CuZr	140	19	215	61	250	19
	15Cu-30NiZr	250	17	310	69	355	14
	30Ni-15CuZr	200	4	235	86	290	10

Table 3: Amount of NH₃ desorbed in NH₃-TPD (mmol NH₃/g_{catalyst})

Group	Catalyst	mmol NH ₃ /g _{cat}
Support	ZrO ₂	0.39
Monometallic	15CuZr	0.18
	15NiZr	1.09
Bimetallic (one-step impregnation)	7Ni7CuZr	1.12
	15Ni7CuZr	0.41
	15Ni15CuZr	0.35
	30Ni15CuZr	0.38
Bimetallic (two-step impregnation)	15Cu-15NiZr	0.38
	15Ni-15CuZr	0.11
	15Cu-30NiZr	0.16
	30Ni-15CuZr	0.17

X-ray diffraction characterization of the catalysts

The XRD patterns for the fresh-reduced and used catalysts are shown in Figures S1, S2 and S3. The reflections detected in these diffraction patterns correspond to Cu⁰ (2θ = 43.4°, 50.5° and 74.2°) and Ni⁰ (2θ = 44.7°, 52.1° and 76.3°). Diffraction peaks ascribed to carbon were detected in the used catalysts (2θ = 35.8°, and 60.1°), which may be related to coke formation under reaction conditions.³³⁻³⁷⁻³⁹ A high peak at 2θ = 35.9° was observed in some used catalysts. This peak was attributed to CSi, which was used to fix the catalytic bed. Moreover, the average Ni and Cu crystallite sizes for these catalysts were calculated by the Scherrer equation, and these data are summarized in Table S1, S2 and S3.

Concerning monometallic catalysts (see Figure S1), the fresh-reduced 15CuZr catalyst registered defined peaks associated with metallic Cu crystallites with a size of 50 nm. After the reaction, they were transformed into small crystallites that could hardly be detected by XRD. A barely noticeable peak can be discerned in the XRD pattern for the freshly reduced 15NiZr catalyst, which can be ascribed to an amorphous structure. Moreover, peaks related to carbon deposition were observed in the used catalyst.

The reduced and used bimetallic 7Ni7CuZr catalyst impregnated in one step did not record any peaks related to Ni⁰ or Cu⁰. This means that this catalyst was composed

mainly of small crystallites before the reaction, and that these crystallites did not recrystallize during the reaction. Similarly, the 15Ni7CuZr catalyst showed a small peak (2θ = 44.7°) that may be related to metallic Ni crystallites with an average size of 20 nm. After the reaction, Ni crystallites were not detectable by XRD (crystallite size < 5 nm). The interaction between Ni and Cu crystallites could not be observed in any of these cases. In contrast, the 15Ni15CuZr catalyst registered a double-peak in both the fresh-reduced and used catalysts at two different positions 2θ = 43 - 44° and at 2θ = 51°, which may be related to Ni-Cu crystallites. A comparison of crystallite size before and after the reaction showed that the size of the Cu-enriched crystallites decreased, while the size of those enriched in Ni increased. This finding suggests that a rearrangement of the crystallites occurred during the reaction, leading to smaller Cu-enriched crystallites and larger Ni-enriched crystallites. Finally, the crystallites observed in the 30Ni15CuZr catalyst were enriched in Ni, decreasing in size from 15 nm to 10 nm after hydrogenolysis reaction. Cu crystallites were not detectable.

The bimetallic 15Cu-15NiZr and 15Ni-15CuZr catalysts impregnated in two steps recorded highly intensive signals ascribed to a Ni-Cu combination. The crystallite size increased slightly in the case of 15Cu-15NiZr, probably due to the sintering of the metallic sites. When adding a higher Ni loading, i.e., 15Cu-30NiZr, the catalyst recorded a similar crystallite size before and after the reaction. This means that the crystallite structure was kept stable during the reaction. In contrast, the crystallites in the 30Ni-15CuZr catalyst grew, probably because of a sintering effect.

To understand the difference in the crystal composition between pure Ni and Cu and bimetallic Ni-Cu, an enlarged graph for the fresh catalysts is reported in Figure S4. The monometallic Cu and Ni registered a diffraction peak at 2θ = 43.4° and 2θ = 44.7°, respectively. The bimetallic catalysts recorded a reflection angle between these two limits, meaning that the crystallites were formed by both Ni and Cu metals. In the case of bimetallic catalysts impregnated in two steps, adding Cu in a first step produced crystallites enriched in Ni. Moreover, impregnating Ni in a first step

provided Cu-enriched crystals. This is consistent with the Ni and Cu loadings measured by ICP-OES.

Morphological characteristics

The elemental maps for the most interesting bimetallic catalysts were obtained by Scanning Transmission Electron Microscopy, which was used to calculate the average size of the metallic particles. The maps for the fresh-reduced catalysts and the value of the average particle size are shown in the Supporting information (Figure S5) and Table 4, respectively. The elemental maps reflected the interaction between Ni and Cu ascribed to bimetallic particles. Moreover, an optimal dispersion of these particles in the support was observed. Regarding the mean particle size, the bimetallic catalysts impregnated in one step recorded a higher particle size than the catalysts impregnated in two steps, and, in this sense, lower particle sizes generally lead to a higher dispersion of active sites. However, the 15Cu-15NiZr catalyst did not follow this tendency; in spite of being synthesized in two steps, it showed similar particle sizes compared to those catalysts prepared in a single impregnation step.

Table 4: Mean particle size for the bimetallic catalysts

Group	Catalyst	Mean particle size (nm)
Bimetallic (one-step impregnation)	15Ni15CuZr	55.5
	30Ni15CuZr	48.6
	15Cu-15NiZr	44.7
Bimetallic (two-step impregnation)	15Ni-15CuZr	22.9
	15Cu-30NiZr	26.9
	30Ni-15CuZr	20.9

Surface properties

The oxidation state of the species formed after catalyst preparation and their atomic ratios were studied by XPS for fresh-reduced and used catalysts. The results are summarized in Table 5. The ratios between the metallic Cu and Ni and their ions were calculated to understand whether the species underwent oxidation or reduction during the reaction. The Ni⁰/Zr ratio was also calculated due to the importance of surface metallic Ni content in the product distribution. Moreover, the deconvolution of the main catalysts is outlined in Figure S6.

A comparison of the monometallic catalysts showed that the 15CuZr catalyst recorded a higher metal-to-Zr ratio than the 15NiZr catalyst, suggesting that a higher amount of surface metal was available in the 15CuZr catalyst. Moreover, the monometallic Cu catalyst recorded a slight decrease in the Cu/Zr ratio after being used in the reaction, presumably owing to the coke deposition on the active sites and/or metal sintering. Coke formation was confirmed by the C/Zr ratio, which was observed to increase after the reaction for all the prepared catalysts. In the case of the monometallic Ni catalyst, the decrease in the metal-

to-support ratio (probably caused by the sintering of Ni particles) and the increase in the C/Zr ratio after hydrogenolysis were more notable, as well as their observation in the XRD results. It is important to note the low Ni⁰/Ni⁺² ratio for the fresh-reduced Ni monometallic catalyst, which was consistent with the H₂-TPR results, where a high reduction temperature was observed. Coke deposition can also be associated with the high acidity⁴⁰ ascribed to the presence of Ni⁺² Lewis acid sites (as shown by the NH₃-TPD results).

The catalysts prepared by one-step impregnation behaved differently depending on the Ni and Cu loading. Both the 7Ni7CuZr catalyst and the 15NiZr catalyst recorded a low Ni⁰/Ni⁺² ratio in the fresh-reduced state. This finding closely matches the H₂-TPR and NH₃-TPD results, whereby these catalysts presented higher reduction temperatures and higher acidities. The used 15NiZr catalyst was completely covered by carbon, according to the high acidity observed in its NH₃-TDP. A high carbon deposition was also observed for the 15Ni7CuZr catalyst. In addition, note should be taken of the high Ni⁰/Zr ratio of the 15Ni15CuZr catalyst, which decreased after the reaction, indicating that Ni was oxidized during the reaction. In this sense, the butanol or water produced as a byproduct during the hydrogenolysis reaction could oxidize the Ni species to NiO during the reaction, as reported previously.⁴¹⁻⁴³ The high Cu/Zr ratio detected in the fresh-reduced catalyst fell sharply after the reaction. Finally, the 30Ni15CuZr catalyst recorded lower metal-to-support ratios, and a decrease in these ratios after the reaction, probably because of the inaccessibility of the metallic sites after being partially covered by carbon deposits. Indeed, a high C/Zr ratio was observed for this catalyst after reaction, which was ascribed to a high coke deposition on its surface.

Concerning the bimetallic catalysts synthesized in two steps, the 15Cu-15NiZr catalyst recorded the highest carbon deposition, which was consistent with its higher acidity (see Table 3). Moreover, this catalyst recorded low metal-to-support ratios before the reaction, which increased after 25 h on stream; this could be explained by the carbon deposition on the catalyst support, implying that less support was accessible after the reaction. A similar effect was observed for the 15Ni-15CuZr catalyst, where higher metal-to-support ratios were obtained in the used catalysts. Moreover, metals were reduced during the reaction. When impregnating a higher amount of Ni (for the 15Cu-30NiZr and 30Ni-15CuZr catalysts), higher Ni/Zr ratios were obtained, which in turn slightly decreased after the reaction. In the case of the reduced 30Ni-15CuZr catalyst, the metal-to-support ratio was higher than that of the 15Cu-30NiZr catalyst. In both cases, Ni⁰/Zr was high at the beginning of the reaction, but Ni was partially oxidized during the reaction, and, therefore, a lower ratio was recorded after the reaction. As explained before, either the solvent or the water produced during the reaction could be the agents responsible for metallic Ni oxidation.

Table 5: XPS results for the monometallic and bimetallic catalysts

Group	Catalyst		Cu/Zr	Cu ^o / (Cu ⁺¹ + Cu ⁺²)	Ni/Zr	Ni ^o /Ni ⁺²	Ni ^o /Zr	C/Zr
Monometallic	15CuZr	Reduced	0.37	1.64				1.12
		Used ^a	0.25	1.28				10.80
Monometallic	15NiZr	Reduced			0.15	0.20	0.03	4.96
		Used ^a			0.07	0.32	0.02	35.68
Bimetallic (one-step impregnation)	7Ni7CuZr	Reduced	0.22	0.39	0.04	0.37	0.01	6.63
		Used ^a	-	-	-	-	-	Only C
	15Ni7CuZr	Reduced	0.27	0.38	0.58	0.79	0.26	63.09
		Used ^a	0.62	0.74	0.35	0.43	0.11	261.68
	15Ni15CuZr	Reduced	1.59	0.33	1.35	0.46	0.42	7.20
		Used ^b	0.28	1.95	1.32	0.32	0.32	20.67
30Ni15CuZr	Reduced	0.51	0.44	0.44	0.78	0.19	4.19	
	Used ^b	0.43	1.08	0.23	0.40	0.07	78.92	
Bimetallic (two-step impregnation)	15Cu-15NiZr	Reduced	0.43	1.32	0.05	0.56	0.02	38.39
		Used ^c	2.56	1.45	0.48	0.55	0.17	126.18
	15Ni-15CuZr	Reduced	0.57	0.43	0.54	0.71	0.23	4.28
		Used ^c	0.77	1.07	0.79	0.92	0.38	51.48
	15Cu-30NiZr	Reduced	1.26	0.93	1.35	1.13	0.71	11.44
		Used ^c	0.61	1.44	1.32	0.39	0.37	18.97
30Ni-15CuZr	Reduced	1.46	1.07	1.46	1.19	0.79	5.15	
	Used ^c	1.20	2.77	1.26	0.40	0.36	49.04	

* Used catalyst operating conditions: T = 275 °C; P_{H₂} = 15 bar; time on stream: ^a 10 h; ^b 24 h; ^c 25 h

Activity results

Monometallic catalysts

The activity results for the monometallic catalysts are summarized in Figure 3. The 15CuZr catalyst underwent a complete HMF conversion, whereas the monometallic Ni catalyst recorded a conversion of over 90 %. The 15CuZr catalyst recorded a DMF yield of approximately 30 %, and was found to be stable after 10 h on stream. In contrast, the 15NiZr catalyst reached a maximum yield of 20 % after 4 h time on stream, but decreased to 10 % after 10 h reaction

time. In both cases, no DMTHF was detected. The better performance of the 15CuZr catalyst could be related to its greater BET area and its better reducibility providing a higher HMF conversion and DMF yield. Moreover, the higher acidity of the 15NiZr catalyst can favor C–C cleavage, producing ring-opening products.⁴⁴ The deactivation of this catalyst could be caused by the coke deposition on the active sites (determined by XPS and XRD characterization techniques) and/or by possible particle sintering (as observed from the data derived from XPS).

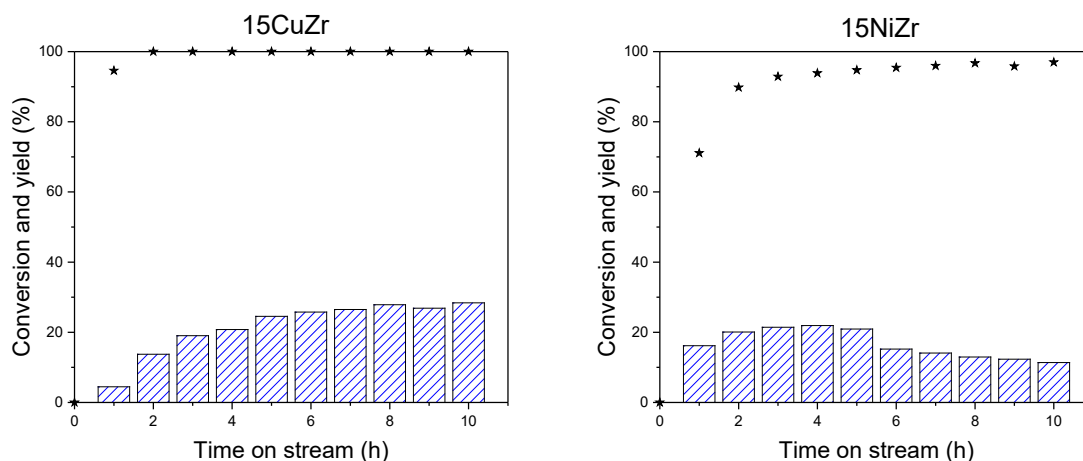




Figure 3: Conversion and yield for the monometallic catalysts (★ HMF conversion,  DMF yield and  DMTHF yield)

Bimetallic catalysts impregnated in one step

The activity results for bimetallic catalysts impregnated in one step are summarized in Figure 4. For the 7Ni7CuZr and 15Ni7CuZr catalysts, the reaction was stopped after 10 h due to the poor total yield and the observed deactivation after 7 h on stream. In both cases, a small amount of DMTHF was detected in the first reaction hours. The high carbon deposition may cover the active metal sites, and, thus, result in the deactivation of the catalysts. In contrast, impregnating higher amounts of Ni and Cu (15Ni15CuZr and 30Ni15CuZr catalysts) provided higher yields for the desired products during 24 h of reaction time (the figures for the conversion and yields at 23 h are the averages for the overall production during the night). The good performance of these catalysts can be attributed to their higher interaction between Cu and Ni metals, as observed in the XRD results. Therefore, there seems to be a close relationship between the DMTHF and DMF yield obtained and the

Ni-Cu interaction formed in each catalyst (Figure 6). The high DMTHF production associated with the 15Ni15CuZr catalyst at the beginning of the reaction (40 % yield of DMTHF at 4 h of reaction time) can be linked to the high metallic Ni content on the surface of the catalyst detected by XPS, which has a high hydrogenation capacity. After the reaction, the catalyst showed some Ni oxidation, which may be responsible for the decrease in the production of DMTHF, which seems to take place through DMF hydrogenation. Finally, the 30Ni15CuZr catalyst recorded a maximum DMF yield of 25 %, which remained almost constant after 24 h of reaction. As regards the aforementioned catalyst, a small production of DMTHF was observed at the beginning of the reaction. This may be due to the smaller amount of metallic Ni observed by XPS and the lower dispersion of the metals due to larger crystallites, compared to the 15Ni15CuZr catalyst.

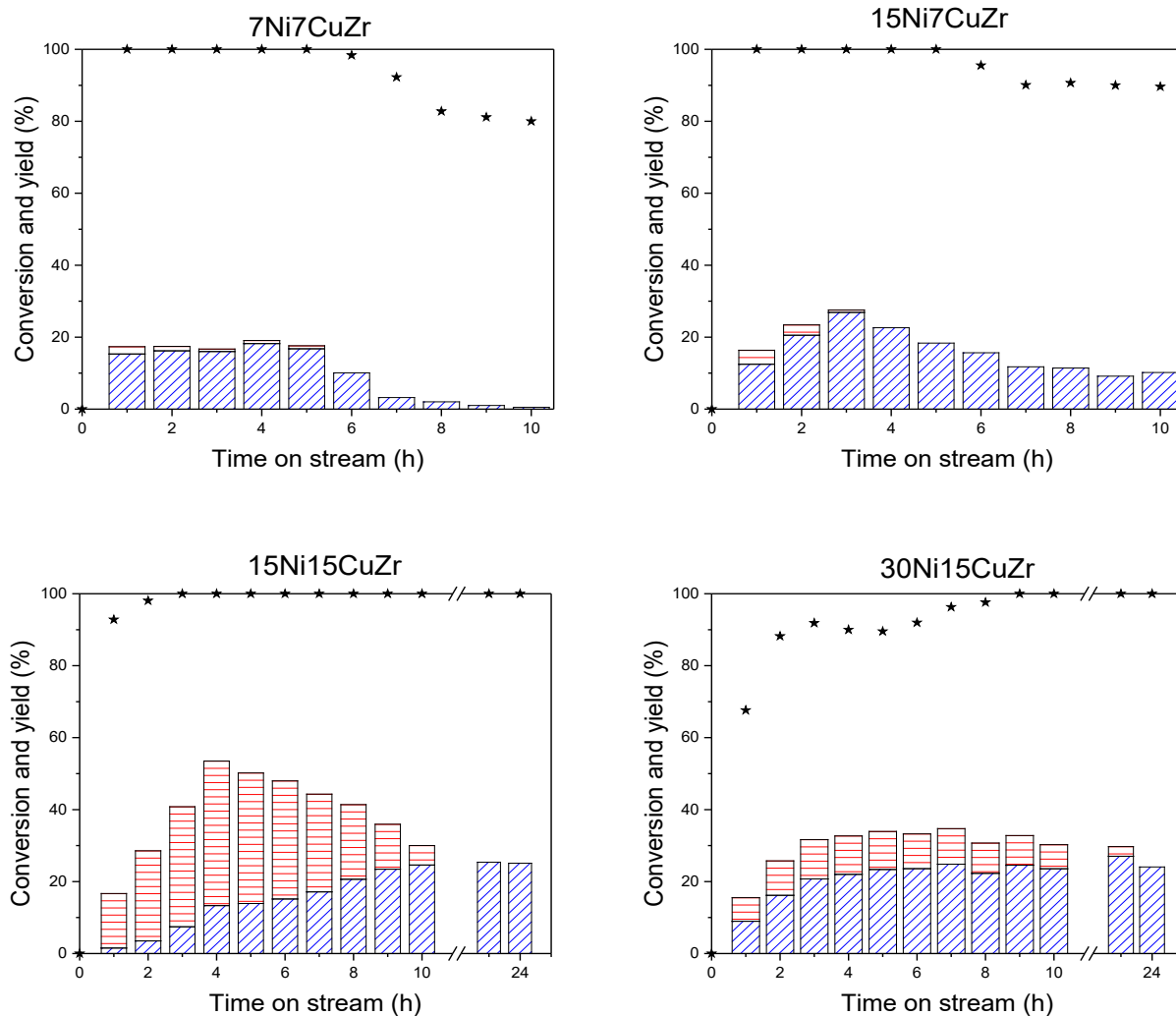



Figure 4: Conversion and yield for the bimetallic catalysts impregnated in one step (★ HMF conversion,  DMF yield and DMTHF yield)

Bimetallic catalysts impregnated in two steps

Figure 5 shows the activity results for the bimetallic catalysts impregnated in two steps. The high production of DMF and DMTHF is probably related to the interaction of Ni and Cu (Figure 6). Moreover, the yields for the desired products are higher than that found for the bimetallic catalysts impregnated in one step. This can be ascribed to the lower particle size of these catalysts. The 15Cu-15NiZr catalyst reached a maximum DMF yield of 50 % after 8 h of time on stream, which then fell to 10 % after 25 h, probably due to the sintering of metal particles and/or coke deposition on the active sites. Furthermore, this catalyst hardly produced any DMTHF. In contrast, the 15Ni-15CuZr catalyst recorded a lower deactivation after 25 h time on stream; reaching a maximum DMF yield of 70 % after 8 h. The higher yield observed in this catalyst may be related to its smaller bimetallic Ni-Cu particles with higher dispersion. In addition, the higher metal-to-support ratio observed by XPS may enhance the production of the desired products.

The 15Cu-30NiZr and 30Ni-15CuZr catalysts recorded high yields of DMTHF. The higher metallic Ni surface content observed by XPS produces higher DMTHF due to the

hydrogenating capacity of Ni.⁴⁵ Both catalysts showed a similar tendency, achieving high DMTHF yields at the first stage of the reaction, and high DMF yields after 23 h of time on stream. As indicated by the results obtained from XPS (see Table 5), Ni was partially oxidized during the reaction, presumably suppressing its DMF hydrogenation capacity and producing DMF instead of DMTHF. However, the 15Cu-30NiZr catalyst recorded a lower DMTHF yield during the reaction. This can be ascribed to the lower Ni/Zr and Cu/Zr ratios observed in XPS; with higher Ni loading implying lower particle size, which resulted in a better dispersion for the catalyst. Additionally, the interaction of Ni-Cu observed in the H₂-TPR profiles became stronger when the Ni loading was increased. These two considerations can explain the better performance of the catalysts with higher Ni loadings.

As noted, there seems to be a close relationship between the Ni-Cu interactions observed in H₂-TPR deconvolution profiles and the maximum yield obtained (the sum of DMF and DMTHF production)

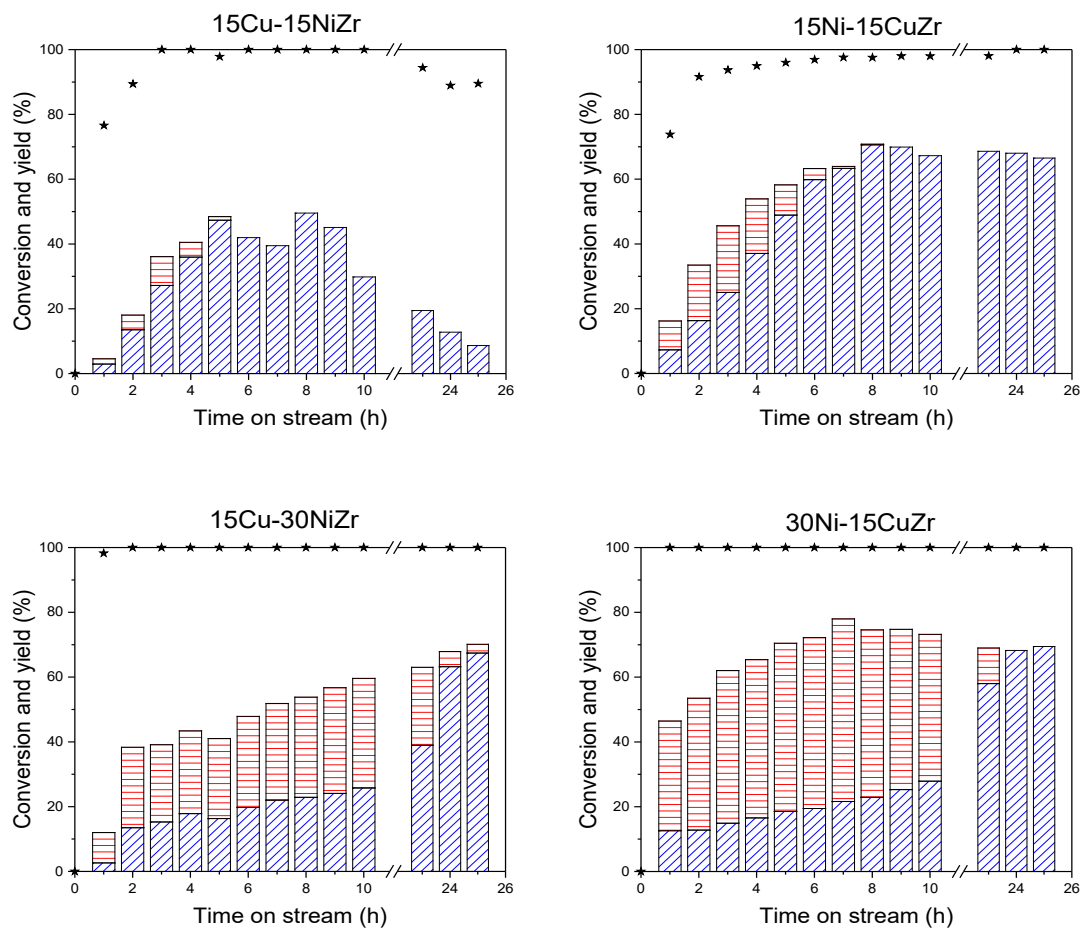




Figure 5: Conversion and yield for the bimetallic catalysts impregnated in two steps (★ HMF conversion,  DMF yield and  DMTHF yield)

Study of the evolution of the catalytic system over the reaction

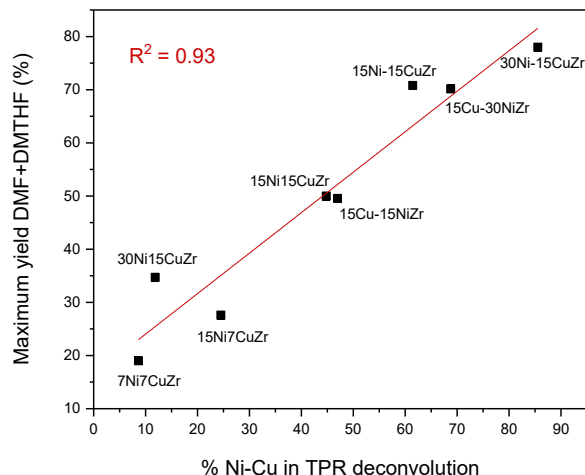


Figure 6: Relation between % Ni-Cu and maximum yield

As discussed above, some catalysts produced DMTHF at the beginning of the reaction, probably due to the presence of Ni metal active sites. However, the lower Ni⁰/Ni²⁺ ratio observed in the used catalysts suggests a progressive Ni oxidation process during the reaction, which decreases the hydrogenation capacity. To confirm these results, different activity tests were carried out by using the 15Cu-30NiZr catalyst for different on stream times (see Table 6). The used catalyst at these different reaction times was then characterized by XRD and XPS techniques to observe the evolution of the catalyst properties.

Table 6: XRD results for the 15Cu-30NiZr catalyst tested

Time on Stream (h)	Cu/Zr	Cu ⁰ /(Cu ⁺¹ + Cu ⁺²)	Ni/Zr	Ni ⁰ /Ni ⁺²	Ni ⁰ /Zr
Fresh-reduced	1.26	0.93	1.35	1.13	0.71
3 h	1.22	1.01	1.34	0.86	0.62
6 h	1.21	0.96	1.26	0.67	0.50
10 h	0.71	0.96	1.22	0.52	0.41
25 h	0.61	1.44	1.02	0.39	0.37

at different reaction times

The XRD results summarized in Table 6 show that the Ni and Cu crystallites followed a similar pattern during the first 10 hours of reaction time, showing a slight decrease in the contribution of the Ni crystallites. This suggests that some Ni crystallites lose some crystallinity during the reaction. After 25 h of reaction time, this decline became more significant. In addition, this trend is comparable to the DMTHF yield profile observed during the activity tests. Specifically, a higher DMTHF yield was observed at the beginning of the reaction, where Ni crystallites remained almost stable, and DMTHF production decreased while Ni crystallites became less crystalline.

Finally, the XPS technique was used to understand the change in the oxidation state of metallic species during the reaction, and the results are summarized in Table 7. In general, a difference is found between the Cu and Ni oxidation-reduction trends. Cu was reduced during the reaction due to the H₂ atmosphere inside the reactor. However, Ni underwent an oxidation process during the reaction, which could be observed from the decrease in the Ni⁰/Zr ratio during the reaction, and may be the reason for the observed decrease in DMTHF production. In fact, when the metallic Ni on the surface was oxidized, its hydrogenating capacity was reduced, which means the hydrogenation process for DMF to produce DMTHF was limited.

Table 7: XPS results for the 15Cu-30NiZr catalyst tested at different reaction times

Time on stream (h)	Crystallite size (nm)		Contribution (%)	
	Cu	Ni	Cu	Ni
Fresh-reduced (0 h)	30	10	16	84
3 h	25	10	15	85
6 h	30	10	20	80
10 h	25	10	22	78
25 h	25	15	44	56

CONCLUSIONS

The catalytic conversion of DMF and DMTHF from HMF was carried out in a continuous fixed-bed reactor. Accordingly, monometallic and bimetallic catalysts were prepared in one or two impregnation steps and then synthesized. The impregnation steps, which were responsible for producing different textural and physico-chemical properties for the bimetallic catalysts, were crucial for the selective hydrogenolysis of HMF to produce DMF or DMTHF.

In general, bimetallic catalysts recorded a better performance and stability than their monometallic counterparts. This is probably due to the presence of the Ni-Cu interaction. In addition, impregnating Ni and Cu metals in sequential steps was found to lead to higher Ni-Cu interaction, smaller particle sizes, and lower acidity. These lower acidity values possibly prevented C-C cleavage and avoided the production of ring-opening products. Moreover, the lower acidity involved less coke deposition, which resulted in lower catalyst deactivation. Another important conclusion is that metallic Ni deposited onto the surface of the catalyst was responsible for DMTHF production. This Ni was partially oxidized during the reaction, leading to a loss in hydrogenating capacity, which limited the hydrogenation step of DMF to DMTHF. Finally, impregnating Ni in a second step involved better reducibility and enhanced dispersion for the metals. Furthermore, higher Ni loading implied a stronger Ni-Cu interaction and better metal dispersion. The 30Ni-15CuZr catalyst, therefore, recorded the best performance, with DMF and DMTHF yields of above 75 %.

ASSOCIATED CONTENT

Supporting Information.

- XRD patterns
- STEM images
- XPS profile deconvolution

This material is available free of charge via the Internet at <http://pubs.acs.org>.

AUTHOR INFORMATION

Corresponding Author

Nerea Viar – Chemical and Environmental Engineering Department. Engineering Faculty of Bilbao, University of Basque Country (UPV/EHU), Plaza Ingeniero Torres Quevedo 1 – 48013 Bilbao (Spain). Email: nerea.viar@ehu.eus

Author Contributions

All the authors contributed to this manuscript.

Funding Sources

This work was supported by the University of the Basque Country (EHU/UPV), the Spanish Ministry of Economy and Innovation and the European Union through the European Regional Development Fund (ERDF) (Projects: RTI2018-094918-B-C43), and the Basque Government (Project: IT993-16)

ACKNOWLEDGMENT

The authors express their gratitude to the General Research Services (SGIker) attached to the EHU/UPV; the university, itself, for its assistance with the SEM analysis, and Pedro J. Maireles (University of Malaga) for his assistance with the XPS results.

REFERENCES

- (1) Dabros, T. M. H.; Stummann, M. Z.; Høj, M.; Jensen, P. A.; Grunwaldt, J. D.; Gabrielsen, J.; Mortensen, P. M.; Jensen, A. D. Transportation Fuels from Biomass Fast Pyrolysis, Catalytic Hydrodeoxygenation, and Catalytic Fast Hydropyrolysis. *Prog. Energy Combust. Sci.* **2018**, *68*, 268–309. DOI 10.1016/j.pecs.2018.05.002.
- (2) Ross, J. R. H. Catalysis in Biomass Conversion. *Contemp. Catal.* **2019**, 343–364. DOI 10.1016/B978-0-444-63474-0.00015-1.
- (3) Han, X.; Guo, Y.; Liu, X.; Xia, Q.; Wang, Y. Catalytic Conversion of Lignocellulosic Biomass into Hydrocarbons: A Mini Review. *Catal. Today* **2019**, *319* (December 2017), 2–13. DOI 10.1016/j.cattod.2018.05.013.
- (4) Bozell, J. J.; Petersen, G. R. Technology Development for the Production of Biobased Products from Biorefinery Carbohydrates - The US Department of Energy's "Top 10" Revisited. *Green Chem.* **2010**, *12* (4), 539–554. DOI 10.1039/b922014c.
- (5) Yu, I. K. M.; Tsang, D. C. W. Conversion of Biomass to Hydroxymethylfurfural: A Review of Catalytic Systems and Underlying Mechanisms. *Bioresour. Technol.* **2017**, *238*, 716–732. DOI 10.1016/j.biortech.2017.04.026.
- (6) Portillo Perez, G.; Mukherjee, A.; Dumont, M. J. Insights into HMF Catalysis. *J. Ind. Eng. Chem.* **2018**, *70*, 1–34. DOI 10.1016/j.jiec.2018.10.002.
- (7) Zhang, L.; Xi, G.; Chen, Z.; Qi, Z.; Wang, X. Enhanced Formation of 5-HMF from Glucose Using a Highly Selective and Stable SAPO-34 Catalyst. *Chem. Eng. J.* **2017**, *307*, 877–883. DOI 10.1016/j.ccej.2016.09.003.
- (8) Solanki, B. S.; Rode, C. V. Selective Hydrogenolysis of 5-(Hydroxymethyl) Furfural over Pd / C Catalyst to 2, 5-Dimethylfuran. *J. Saudi Chem. Soc.* **2018**. DOI 10.1016/j.jscs.2018.08.009.
- (9) Yang, P.; Cui, Q.; Zu, Y.; Liu, X.; Lu, G.; Wang, Y. Catalytic Production of 2,5-Dimethylfuran from 5-Hydroxymethylfurfural over Ni/Co₃O₄ Catalyst. *CATCOM* **2015**, *66*, 55–59. DOI 10.1016/j.catcom.2015.02.014.
- (10) Wang, X.; Liang, X.; Li, J.; Li, Q. Catalytic Hydrogenolysis of Biomass-Derived 5-Hydroxymethylfurfural To. *Appl. Catal. A, Gen.* **2019**, *576* (March), 85–95. DOI 10.1016/j.apcata.2019.03.005.
- (11) Li, T.; Sergio, S.; Ong, G.; Zhang, J.; Jia, C.; Sun, J.; Wang, Y.; Lin, H. One-Pot Conversion of Carbohydrates into Furan Derivatives in Biphasic Tandem Catalytic Process. *Catal. Today* **2018**, No. November, 0–1. DOI 10.1016/j.cattod.2018.11.052.
- (12) Gao, Z.; Li, C.; Fan, G.; Yang, L.; Li, F. Environmental Nitrogen-Doped Carbon-Decorated Copper Catalyst for Highly Efficient Transfer Hydrogenolysis of 5-Hydroxymethylfurfural to Convertibly Produce. *Appl. Catal. B Environ.* **2018**, *226* (October 2017), 523–533. DOI 10.1016/j.apcatb.2018.01.006.
- (13) Priezel, P.; Endot, N. A.; Cara, P. D.; Lopez-sanchez, J. A. Fast Catalytic Hydrogenation of 2, 5-Hydroxymethylfurfural to 2, 5-Dimethylfuran with Ruthenium on Carbon Nanotubes. **2018**. DOI 10.1021/acs.iecr.7b04715.
- (14) Li, D.; Liu, Q.; Zhu, C.; Wang, H.; Cui, C.; Wang, C.; Ma, L. Selective Hydrogenolysis of 5-Hydroxymethylfurfural to 2,5-Dimethylfuran over Co₃O₄ Catalyst by Controlled Reduction. *J. Energy Chem.* **2019**, *30*, 34–41. DOI 10.1016/j.jechem.2018.03.008.
- (15) Ledesma, B.; Juárez, J.; Mazarío, J.; Domine, M.; Beltramone, A. Bimetallic Platinum / Iridium Modified Mesoporous Catalysts Applied in the Hydrogenation of HMF. *Catal. Today* **2019**, No. February, 1–10. DOI 10.1016/j.cattod.2019.06.037.
- (16) Kong, X.; Zhu, Y.; Zheng, H.; Li, X.; Zhu, Y.; Li, Y. Ni Nanoparticles Inlaid Nickel Phyllosilicate as a Metal – Acid Bifunctional Catalyst for Low-Temperature Hydrogenolysis Reactions. **2015**. DOI 10.1021/acscatal.5b01080.
- (17) Kumalaputri, A. J.; Bottari, G.; Erne, P. M.; Heeres, H. J.; Barta, K. Tunable and Selective Conversion of 5-HMF to 2, 5-Furandimethanol and 2, 5-Dimethylfuran over Copper-Doped Porous Metal Oxides. **2014**, 2266–2275. DOI 10.1002/cssc.201402095.
- (18) Pastor-Pérez, L.; Gu, S.; Sepúlveda-Escribano, A.; Reina, T. R. Bimetallic Cu–Ni Catalysts for the WGS Reaction – Cooperative or Uncooperative Effect? *Int. J. Hydrogen Energy* **2019**, *44*. DOI 10.1016/j.ijhydene.2018.12.127.
- (19) Viar, N.; Reques, J. M.; Agirre, I.; Iriondo, A.; Arias, P. L. Furanic Biofuels Production from Biomass Using Cu-Based Heterogeneous Catalysts. *Energy* **2019**, *172*, 531–544. DOI 10.1016/j.energy.2019.01.109.
- (20) Khzouz, M.; Gkanas, E. I.; Du, S.; Wood, J. Catalytic Performance of Ni-Cu/Al₂O₃ for Effective Syngas Production by Methanol Steam Reforming. *Fuel* **2018**, *232* (January 2017), 672–683. DOI 10.1016/j.fuel.2018.06.025.
- (21) Pongsombate, A.; Imyen, T.; Dittanet, P.; Embley, B.; Kongkachuichay, P. Direct Synthesis of Dimethyl Carbonate from CO₂ and Methanol by Supported Bimetallic Cu–Ni/ZIF-8 MOF Catalysts. *J. Taiwan Inst. Chem. Eng.* **2017**, *80*, 16–24. DOI 10.1016/j.jtice.2017.07.019.
- (22) Li, X.; Xiang, M.; Wu, D. Hydrogenolysis of Glycerol over Bimetallic Cu e Ni c Atalysts Supported on Hierarchically Porous SAPO-11 Zeolite. *Catal. Commun.* **2019**, *119* (November

- 2018), 170–175. DOI 10.1016/j.catcom.2018.11.004.
- (23) Requies, J. M.; Frias, M.; Cuezva, M.; Iriondo, A.; Agirre, I.; Viar, N. Hydrogenolysis of 5-Hydroxymethylfurfural To Produce 2,5-Dimethylfuran over ZrO₂ Supported Cu and RuCu Catalysts. *Ind. Eng. Chem. Res.* **2018**, *57* (34), 11535–11546. DOI 10.1021/acs.iecr.8b01234.
- (24) Pérez-Hernández, R.; Gutiérrez-Martínez, A.; Espinosa-Pesqueira, M. E.; Estanislao, M. L.; Palacios, J. Effect of the Bimetallic Ni/Cu Loading on the ZrO₂ support for H₂ production in the Autothermal Steam Reforming of Methanol. *Catal. Today* **2015**, *250*, 166–172. DOI 10.1016/j.cattod.2014.08.009.
- (25) Jia, X.; Zhang, X.; Rui, N.; Hu, X.; Liu, C. Applied Catalysis B: Environmental Structural Effect of Ni / ZrO₂ Catalyst on CO₂ Methanation with Enhanced Activity. *Appl. Catal. B Environ.* **2019**, *244* (November 2018), 159–169. DOI 10.1016/j.apcatb.2018.11.024.
- (26) López, P.; Mondragón-Galicia, G.; Espinosa-Pesqueira, M. E.; Mendoza-Anaya, D.; Fernández, M. E.; Gómez-Cortés, A.; Bonifacio, J.; Martínez-Barrera, G.; Pérez-Hernández, R. Hydrogen Production from Oxidative Steam Reforming of Methanol: Effect of the Cu and Ni Impregnation on ZrO₂ and Their Molecular Simulation Studies. *Int. J. Hydrogen Energy* **2012**, *37* (11), 9018–9027. DOI 10.1016/j.ijhydene.2012.02.105.
- (27) Yoshida, R.; Sun, D.; Yamada, Y.; Sato, S.; Hutchings, G. J. Vapor-Phase Hydrogenation of Levulinic Acid to γ -Valerolactone over Cu-Ni Bimetallic Catalysts. *Catal. Commun.* **2017**, *97* (March), 79–82. DOI 10.1016/j.catcom.2017.04.018.
- (28) Cai, F.; Pan, D.; Ibrahim, J. J.; Zhang, J.; Xiao, G. Hydrogenolysis of Glycerol over Supported Bimetallic Ni/Cu Catalysts with and without External Hydrogen Addition in a Fixed-Bed Flow Reactor. *Appl. Catal. A Gen.* **2018**, *564* (April), 172–182. DOI 10.1016/j.apcata.2018.07.029.
- (29) Torres, D.; Pinilla, J. L.; Suelves, I. Screening of Ni-Cu Bimetallic Catalysts for Hydrogen and Carbon Nano Filaments Production via Catalytic Decomposition of Methane. *Appl. Catal. A, Gen.* **2018**, *559* (April), 10–19. DOI 10.1016/j.apcata.2018.04.011.
- (30) Yang, Z.; Liu, Y.; Li, Y.; Zeng, L.; Liu, Z.; Liu, X.; Liu, C. Effect of Preparation Method on the Bimetallic NiCu/SAPO-11 Catalysts for the Hydroisomerization of n-Octane. *J. Energy Chem.* **2019**, *28*, 23–30. DOI 10.1016/j.jechem.2017.10.003.
- (31) Alamillo, R.; Tucker, M.; Chia, M.; Pagán-Torres, Y.; Dumesic, J. The Selective Hydrogenation of Biomass-Derived 5-Hydroxymethylfurfural Using Heterogeneous Catalysts. *Green Chem.* **2012**, *14* (5), 1413–1419. DOI 10.1039/c2gc35039d.
- (32) Iriondo, A.; Mendiguren, A.; Güemez, M. B.; Requies, J.; Cambra, J. F. 2,5-DMF Production through Hydrogenation of Real and Synthetic 5-HMF over Transition Metal Catalysts Supported on Carriers with Different Nature. *Catal. Today* **2017**, *279*, 286–295. DOI 10.1016/j.cattod.2016.02.019.
- (33) Yang, Z.; Liu, Y.; Liu, D.; Meng, X.; Liu, C. Hydroisomerization of N-Octane over Bimetallic Ni-Cu/SAPO-11 Catalysts. *Appl. Catal. A Gen.* **2017**, *543* (June), 274–282. DOI 10.1016/j.apcata.2017.06.028.
- (34) Fu, Z.; Wang, Z.; Lin, W.; Song, W.; Li, S. High Efficient Conversion of Furfural to 2-Methylfuran over Ni-Cu/Al₂O₃ catalyst with Formic Acid as a Hydrogen Donor. *Appl. Catal. A Gen.* **2017**, *547* (June), 248–255. DOI 10.1016/j.apcata.2017.09.011.
- (35) Li, J.; Li, T.; Ma, H.; Sun, Q.; Ying, W.; Fang, D. Effect of Nickel on Phosphorus Modi Fi Ed HZSM-5 in Catalytic Cracking of Butene and Pentene. *Fuel Process. Technol.* **2017**, *159*, 31–37. DOI 10.1016/j.fuproc.2016.06.034.
- (36) Ye, R.; Gong, W.; Sun, Z.; Sheng, Q.; Shi, X.; Wang, T.; Yao, Y.; Razink, J. J.; Lin, L.; Zhou, Z.; Adidharma, H.; Tang, J.; Fan, M.; Yao, Y. Enhanced Stability of Ni / SiO₂ Catalyst for CO₂ Methanation: Derived from Nickel Phyllosilicate with Strong Metal-Support Interactions. *Energy* **2019**, *188*, 116059. DOI 10.1016/j.energy.2019.116059.
- (37) Srivastava, S.; Jadeja, G. C.; Parikh, J. Journal of Molecular Catalysis A: Chemical Synergism Studies on Alumina-Supported Copper-Nickel Catalysts towards Furfural and 5-Hydroxymethylfurfural Hydrogenation. *Journal Mol. Catal. A, Chem.* **2017**, *426*, 244–256. DOI 10.1016/j.molcata.2016.11.023.
- (38) Freitas, I. C.; Manfro, R. L.; Souza, M. M. V. M. Applied Catalysis B: Environmental Hydrogenolysis of Glycerol to Propylene Glycol in Continuous System without Hydrogen Addition over Cu-Ni Catalysts. *Applied Catal. B, Environ.* **2018**, *220*, 31–41. DOI 10.1016/j.apcatb.2017.08.030.
- (39) Kleebusch, E.; Patzig, C.; Höche, T.; Rüssel, C. Agent - Crystallization and Microstructure Studied by XRD and (S) TEM-EDX. **2018**, *44* (February), 19818–19824. DOI 10.1016/j.ceramint.2018.07.239.
- (40) Jiao, Y.; Zhang, H.; Li, S.; Guo, C.; Yao, P.; Wang, J. Impact of Acidity in ZrO₂-TiO₂-Al₂O₃ Composite Oxides on the Catalytic Activity and Coking Behaviors during n-Decane Cracking. *Fuel* **2018**, *233* (May), 724–731. DOI 10.1016/j.fuel.2018.06.011.
- (41) Chimentão, R. J.; Miranda, B. C.; Ruiz, D.; Gispert-guirado, F.; Medina, F.; Llorca, J.; Santos, J. B. O. Catalytic Performance of Zinc-Supported Copper and Nickel Catalysts in the Glycerol Hydrogenolysis. **2020**, *42*, 185–194. DOI 10.1016/j.jechem.2019.07.003.
- (42) Goyal, R.; Sarkar, B.; Bag, A.; Siddiqui, N.; Dumbre, D.; Lucas, N.; Kumar, S.; Bordoloi, A.; Bhargava, S. K.; Bordoloi, A. Studies of Synergy between Metal - Support Interfaces and Selective Hydrogenation of HMF to DMF in Water. *J. Catal.* **2016**, *340*, 248–260. DOI 10.1016/j.jcat.2016.05.012.
- (43) Ballesteros-Plata, D.; Infantes-Molina, A.; Rodríguez-Cuadrado, M.; Rodríguez-Aguado, E.; Braos-García, P.; Rodríguez-Castellón, E. Incorporation of Molybdenum into Pd and Pt Catalysts Supported on Commercial Silica for Hydrodeoxygenation Reaction of Dibenzofuran. *Appl. Catal. A, Gen.* **2017**, *547* (May), 86–95. DOI 10.1016/j.apcata.2017.08.034.
- (44) El, I.; Rhadfi, T.; Atlamsani, A.; Quisefit, J. Chemical K-10 Montmorillonite: An Efficient and Reusable Catalyst for the Aerobic C C Bond Cleavage of α -Substituted Ketones. *Journal Mol. Catal. A, Chem.* **2012**, *363–364*, 437–445. DOI 10.1016/j.molcata.2012.07.022.
- (45) Huang, Y.; Chen, M.; Yan, L.; Guo, Q.; Fu, Y. Nickel - Tungsten Carbide Catalysts for the Production of 2, 5-Dimethylfuran from Biomass-Derived Molecules. **2014**, 1068–1070. DOI 10.1002/cssc.201301356.

For Table of Content Use Only

The oxidation of metallic Ni is the limiting step in the hydrogenation of DMF to DMTHF, which are green biofuels that have the potential to replace conventional gasoline.

